Research Square

Preprints are preliminary reports that have not undergone peer review.
They should not be considered conclusive, used to inform clinical practice,
or referenced by the media as validated information.

Dynamic Response of Helical Gear Pairs Under Random Speed Excitation

Shaopeng Guan
Hebei University of Engineering
Jiaxing Pei
tbve_kr@163.com

Hebei University of Engineering
LeiLei Wang
Hebei University of Engineering
Hongjuan Hou
Hebei University of Engineering
Lingwei Kong
Hebei Hengong Precision Equipment Co., LTD
Yipeng Zhao
Hebei University of Engineering
Ruisheng Hou
Hebei University of Engineering
Jianing Cao
Hebei University of Engineering

Research Article

Keywords: Random rotational speed, Dynamic response, K-L expansion, Normal distribution

Posted Date: March 3rd, 2026

DOI: https://doi.org/10.21203/rs.3.rs-8879793/v1

License: This work is licensed under a Creative Commons Attribution 4.0 International License.
Read Full License

Additional Declarations: No competing interests reported.

Dynamic Response of Helical Gear Pairs Under Random Speed Excitation

ShaopengGuan[a], JiaxingPei[a], LeiLei Wang[a] Hongjuan Hou[a], Lingwei Kong[b], Yipeng Zhao[a], Ruisheng Hou[a], Jianing Cao[a]

[a] *School of Mechanical and Equipment Engineering, Hebei University of Engineering, Handan 056038, China*
[b]*Hebei Hengong Precision Equipment Co., LTD, Handan 056038, China*

Abstract

Helical gear systems are sometimes subjected to random speed excitations in engineering applications, such as gear pairs in wind turbine drivetrains. To investigate the dynamic characteristics of helical gears under random-speed excitation, a dynamic analysis approach is developed. Firstly, the mesh stiffness of the helical gear pair is calculated in the spatial domain using the slicing method combined with the potential energy approach. Subsequently, the K－L expansion is employed to describe the random speed process, According the random rotation speed, the meshing stiffness is transformed into time domain. Finally, a six-degree-of-freedom nonlinear dynamic model of the helical gear pair, incorporating radial, axial, and torsional motions, is established. The vibration responses of a gear pair under random-speed excitations are investigated using Monte Carlo simulations (MCS). The results show that the radial displacement consistently exceeds the axial displacement. The radial displacement exhibits a multimodal distribution, whereas the axial displacement remains more concentrated and approximately symmetric, with only slight changes in its distribution shape across time instants. As the random process's correlation increases, the system response becomes more correlated, revealing stronger statistical coupling. The findings provide a theoretical basis for elucidating the nonstationary dynamic mechanisms of helical gear pairs under random speed excitations.
Keywords: Random rotational speed; Dynamic response; K-L expansion; Normal distribution

1. Introduction

In mechanical transmission systems, the rotational speed of gears is affected by multiple factors, including load fluctuations, control system disturbances, and external environmental influences, exhibiting randomness and nonstationary characteristics more or less. Random speed excitation disrupts the ideal periodicity of the meshing process, thereby introducing time-dependent mesh-stiffness modulation and a non-deterministic system response that cannot be well captured by deterministic models. Accordingly, mesh-stiffness modulation and the associated dynamic behaviour in helical-gear meshes under random speed excitation remain insufficiently understood.

Meshing stiffness is a key parameter governing the dynamic behavior of gear transmissions and is a major source of internal excitation. It plays an important role in shaping vibration responses, load sharing, and meshing impacts. Consequently, extensive research has been conducted worldwide on the modeling and computation of helical gear meshing stiffness. Existing studies have developed a wide range of approaches, including analytical formulations based on tooth compliance and energy methods stiffness evaluation, and contact models incorporating tooth-surface deformation, misalignment, and manufacturing errors. Shuai Mo et al.[1] established a mesh coordinate system based on the tooth-flank geometry of helical gears. The mesh stiffness was subsequently obtained through radial- and profile-wise slicing combined with an energy-based formulation. Zhen Liu et al.[2] proposed a TCA-based framework for spiral bevel gear pairs, where slicing discretisation and contact points defined on the rolling-angle surface were used to evaluate the mesh stiffness. Guimian Liu et al. [3] derived the time-dependent mesh stiffness by incorporating the propagation rate of a tooth-root crack. They further proposed a spur-gear dynamic model capable of capturing large-amplitude vibrations in nonlinear analyses. Wang Yanan et al. [4] investigated the meshing behaviour of spiral bevel gear pairs using a slice-based representation. The mesh stiffness was obtained from analytical expressions and incorporated into a dynamic framework, showing that crack-induced impacts display a clear periodic pattern. Feng M. et al. [5] adopted a slicing-based scheme to reconstruct the helical-gear TVMS by cumulatively assembling the stiffness contributions derived from spur-gear TVMS results.

* Corresponding author.
E-mail address: tbve_kr@163.com(J. Pei)

They further performed a systematic parametric study, examining the effects of helix angle and face width on meshing behaviour. Wang Q. et al. [6] proposed a model for the analysis of helical presented a helical-gear mesh-stiffness analysis model that explicitly includes tooth-profile deviations and assembly errors. Xiaolin Tang et al. [7] examined how single- and double-tooth contact affects mesh stiffness in spur and helical gear meshes, based on an integrated potential-energy formulation. Fei Liu et al. [8] proposed a point-contact transmission approach for calculating mesh stiffness to analyse the plastic response of helical gears with metallic screw transmission. Their results showed that no stable stiffness value exists during transmission, regardless of whether single- or double-tooth engagement occurs. Rezaei M. et al. [9] coupled spur-gear and planetary-gear transmissions to evaluate the mesh stiffness of planetary spur-gear meshes, and reported that the mesh-frequency ratio governs the number of meshing cycles per revolution of the planet gear. Woo-Jin Chung et al. [10] evaluated the helical-gear TVMS and load-sharing transmission error (LSTE) by incorporating the instantaneous pressure angle. A systematic parametric study was then conducted to quantify the influence of helix angle, base-circle radius, and root-circle radius on the stiffness behaviour. Liu C. et al. [11] proposed a prediction method for TVMS based on gear accuracy grades, accounting for manufacturing errors, assembly deviations, and profile modifications. Pedro Marques et al. [12] developed an analytical model derived from the ISO 6336 standard, incorporating maximum tooth stiffness and a parabolic distribution along the tooth length, to evaluate mesh stiffness and load distribution. Wang Le et al. [13] refined the potential energy method by transforming stiffness parameters into the helical gear domain, enabling the calculation of time-varying mesh stiffness (TVMS). Wang Zhengbing et al. [14] developed a static model to evaluate the mesh stiffness of helical gears using an equivalent approximation approach. The model accounts for variations in contact line geometry and single-tooth unit-meshing and was further extended to incorporate tooth-breakage faults for analysing fault-induced mesh stiffness under quasi-static conditions. Huang Kaisheng et al. [15] simplified the wheel body of spur gears into a curved-edge trapezoidal form and improved the Ishikawa method to enhance the accuracy of mesh stiffness computation. The primary objective of the aforementioned studies has been to refine and extend methodologies for evaluating gear mesh stiffness. Most existing studies on helical gear meshing stiffness have been conducted under constant-speed conditions, and the associated modeling and analysis approaches are relatively mature. For variable-speed operation, Pei et al formulated a dynamic framework to examine the coupled vibration behaviour and lubrication performance of a meshing gear pair under time-varying rotational speed. However, the influence of random speed variation on the evolution of meshing stiffness has received much less attention, and corresponding modeling and computational approaches remain to be further explored.

The mesh stiffness varies over the meshing cycle and enters the governing equations as a parametric excitation. Such stiffness variations may lead to vibration amplification and even dynamic instability. Consequently, the dynamics of geared transmissions have been extensively investigated. Gear transmission systems constitute a representative class of nonlinear dynamic systems. A large body of experimental and theoretical work has examined vibration mechanisms, dynamic response behaviour, and modelling strategies for geared transmissions. Kahraman et al. [16] incorporated backlash and static transmission error, assumed constant mesh stiffness, and formulated a single-DOF dynamic model to assess system stability. Blankenship and Kahraman [17] experimentally validated the complex nonlinear vibration characteristics of gear systems with backlash. Cheng et al. [18] established a gear dynamic model incorporating mesh stiffness and damping to analyse the system's vibration response. Wu et al. [19] proposed a gear dynamic analysis model incorporating tooth-crack effects, and examined how crack propagation alters the vibration response of geared transmissions. Yi et al. [20] proposed a nonlinear dynamic model that accounts for pressure-angle variation and bearing-induced backlash. They further identified the critical conditions leading to the onset of chaotic response. Cao et al. [21] formulated a nonlinear dynamic model incorporating load-dependent mesh stiffness, reverse backlash, and tooth-profile deviations. Zhang Y. et al. [22] developed a dynamic model for a multi-shaft helical gear – rotor system. Through eigenvalue analysis and modal superposition, they evaluated its modal properties and corresponding forced-response behaviour. Velex P. et al. [23] investigated the effects of tooth surface friction on the dynamic behaviour of spur and helical gears based on a finite element model. A time-step integration scheme combined with multiple iterative algorithms was employed to satisfy normal and tangential contact conditions during dynamic equation solution. Wang C. et al. [24] established a dynamic model for double-helical gears that accounts for axial vibration, meshing clearance, and axial coupling. Yavuz et al. [25] developed a dynamic model for transmission systems incorporating both parallel-axis and crossed-axis gears, demonstrating that nonlinear modelling approaches are essential when helical gears are coupled with spur or spiral bevel

gears. Jiang H. et al. [26] introduced an improved friction-excitation modelling approach and characterised the time-dependent evolution of the helical-gear contact-line length. Based on this, they constructed a time-varying friction model to assess the resulting dynamic response. Pengfei Yan et al. [27] proposed a method to optimise uneven load distribution in helical gears by dynamically modifying tooth width. The optimal modification parameters obtained from this approach effectively reduced oscillation phenomena and improved load uniformity. Chen, J. et al. [28] formulated a nonlinear dynamic model for helical-gear pairs that incorporates time-dependent mesh clearance induced by hybrid profile modification. Optimisation of multiple modification parameters was shown to significantly reduce the amplitude of chaotic vibrations. Liu, M. et al. [29] proposed a thermo-elastohydrodynamic lubrication (TEHL) model for helical gear pairs, revealing the influence of rotational speed on their dynamic behaviour and tribological performance. Mo, G. et al. [30] formulated a nonlinear dynamic model of a flexibly supported helical cylindrical geared system, incorporating coupled dynamic friction – backlash effects and surface roughness. They further performed a systematic parametric analysis to examine how key control parameters affect the system response. Liu Lei et al. [31] developed a translational – torsional coupled dynamic model for gear systems that accounts for regular meshing forces and meshing stiffness. They analysed the influence of tooth curvature on the system dynamics. Zhang Liu et al. [32] established nonlinear dynamic equations for a helical gear system with bending-torsional shaft coupling, accounting for time-varying meshing stiffness and pitch error, and investigated the effects of stiffness variation and pitch error on system vibration characteristics. Despite growing interest in the dynamics of geared transmissions subjected to variable-speed excitation, most studies assume a deterministic rotational speed. It fails to fully capture the transient meshing effects induced by random speed fluctuations.

This paper presents a framework for computing the mesh stiffness and analysing the nonlinear dynamics of helical gears subjected to random rotational-speed excitation. First, the helical gear is discretised across the face width using the slicing approach. The mesh stiffness of each slice is evaluated via a potential-energy-based formulation, and the global time-dependent stiffness of the helical gear pair is then obtained by numerically integrating the slice contributions. Second, random rotational speed signals are generated using the K-L expansion, and the corresponding time-varying meshing stiffness under stochastic speed conditions is determined. Subsequently, a nonlinear dynamic model of the helical gear pair is established by comprehensively considering static transmission error, backlash, and nonlinear mesh force to analyze the vibration displacement distribution at different stochastic time instants. Finally, the dynamic responses obtained under multiple stochastic rotational-speed scenarios are analysed statistically to quantify how random speed excitation affects vibration behaviour.

2. The model

2.1. Engagement stiffness

For helical gear pairs, the contact line becomes inclined when the engagement switches from single-tooth to double-tooth contact, causing the mesh stiffness to vary significantly over time and along the contact line. A coupled modelling strategy is established, where the gear mesh is discretised by slicing, and the stiffness of each slice is derived using the potential energy method. The equivalent mesh stiffness of the helical-gear pair is subsequently obtained via superposition of all slice-wise contributions.

As depicted in Fig. 1, the helical gear is partitioned across the face width into a series of slices, each represented by an equivalent spur-gear pair. The meshing stiffness of each slice is evaluated via a potential-energy-based formulation. The slice-wise stiffness contributions are then assembled along the line of action to yield the global time-dependent mesh stiffness of the helical gear pair.

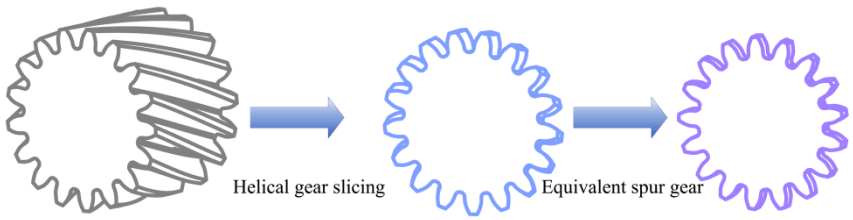


Fig. 1. Equivalent slice of helical gear.

A helical gear is discretized in the face-width direction using the slicing approach, and each segment is modelled as an equivalent spur-gear engagement. A potential-energy-based formulation is employed to evaluate the mesh stiffness of each equivalent spur-gear slice at each time instant. As illustrated in Fig. 2, the meshing principle of spur gears describes the correspondence between the load transfer along the line of action and the elastic deformation of the tooth surface for a single tooth pair:

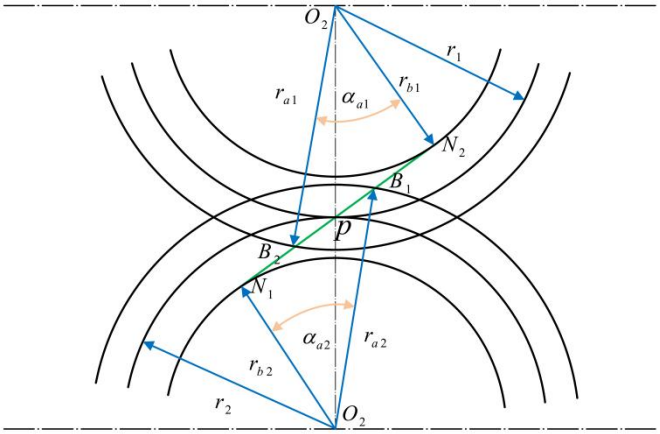


Fig. 2. Principle of straight gear meshing.

where, point P is the point of contact between the two spur gears; B_1 and B_2 are the actual entry point and exit point of the spur gear; N_1 and N_2 are the theoretical entry point and exit point of a spur gear; $r_{a1,2}$ is the tooth tip radius; $r_{1,2}$ is the radius of the pitch circle; $r_{b1,2}$ is the base circle radius of a spur gear; O_1 and O_2 represent the center positions of the drive and driven gears; $\alpha_{1,2}$ is the maximum pressure angle between the bite-out point and the bite-in point.

As shown in Fig. 3, the equivalent spur-gear slice is idealised as a cantilever beam with a non-uniform cross-section.

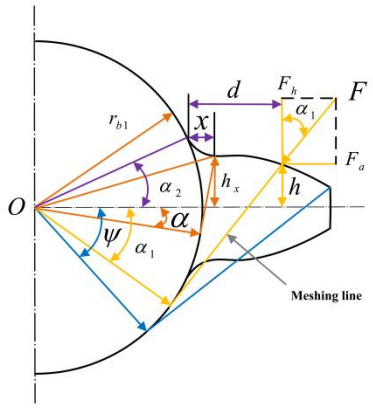


Fig. 3. Gear cantilever beam model.

During helical gear meshing, the line of contact exhibits different spatial distributions over a complete engagement cycle of a single tooth, depending on the relative magnitudes of the transverse and axial contact ratios. Consequently, two distinct approaches can be used to describe and calculate the line of contact.

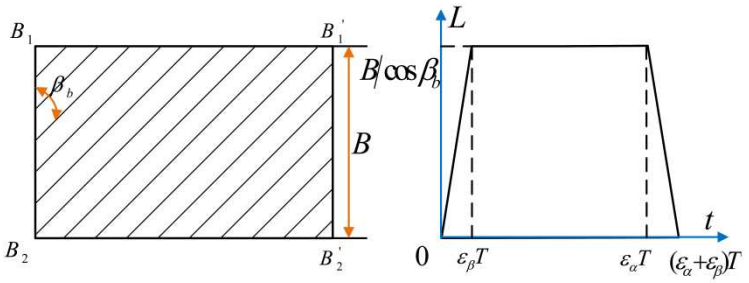


Fig. 4. Time-varying meshing line length $\varepsilon\alpha>\varepsilon\beta$.

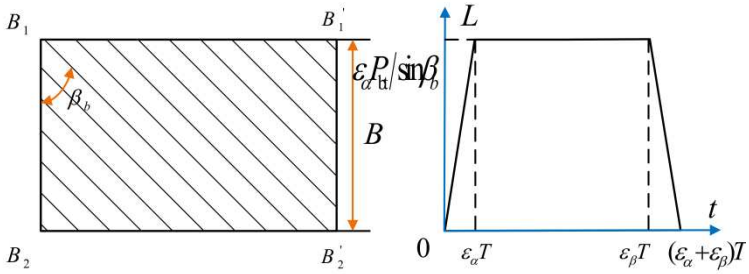


Fig. 5. Time-varying meshing line length $\varepsilon\alpha<\varepsilon\beta$.

In a helical-gear mesh, the maximum single-tooth contact-line length is denoted by L_{max}:

$$L_{max}=\begin{cases}B/\cos\beta_b & \varepsilon_\alpha>\varepsilon_\beta\\ \varepsilon_\alpha P_{bt}/\sin\beta_b & \varepsilon_\alpha<\varepsilon_\beta\end{cases} \tag{1}$$

The length of the tooth contact line for any given engagement time is L:

$$L=\begin{cases}L_{max}/(\varepsilon_1 t_z)t & t\in[0,\varepsilon_1 t_z]\\ L_{max} & t\in[\varepsilon_1 t_z,\varepsilon_2 t_z]\\ L_{max}/\varepsilon_1(\varepsilon_1+\varepsilon_2-t/t_z) & t\in[\varepsilon_1 t_z,(\varepsilon_1+\varepsilon_2)t_z]\end{cases} \tag{2}$$

where $\varepsilon_1=\min(\varepsilon_\alpha,\varepsilon_\beta)$, $\varepsilon_2=\max(\varepsilon_\alpha,\varepsilon_\beta)$. ε_α represent the face concentricity of the helical gears; ε_β represents the axial concentricity of the helical gears.

Helical gear meshes exhibit a continuously changing contact state across the face width as engagement progresses. To accurately characterise this spatial-meshing behaviour, it is necessary to transform the potential-energy-based stiffness parameters of spur gears into the equivalent stiffness-parameter framework of helical gears. The mesh stiffness of a helical gear pair consists of five components: K_h, K_b, K_s, K_a, and K_f denote the Hertzian contact stiffness, bending stiffness, shear stiffness, axial compression stiffness, and foundation stiffness, respectively[33]:

$$\frac{1}{k_h}=\frac{2U_h}{F^2}=\frac{4\left(1-\nu^2\right)}{\pi EB} \tag{3}$$

$$k_b=\sum_{i=1}^{N}1\Big/\left(\int_{-\alpha_1}^{\alpha_2}\frac{3(\alpha_2-\alpha)\cos\alpha}{[\sin\alpha+(\alpha_2-\alpha)\cos\alpha]^3}\times\frac{\left\{1+\cos\alpha_1'[(\alpha_2-\alpha)\sin\alpha-\cos\alpha]\right\}^2}{2E\Delta y}d\alpha\right) \tag{4}$$

$$k_s=\sum_{i=1}^{N}\frac{1}{\int_{-\alpha_1}^{\alpha_2}\frac{1.2(1+\nu)(\alpha_2-\alpha)\cos\alpha\cos^2\alpha_1}{E[\sin\alpha+(\alpha_2-\alpha)\cos\alpha]\Delta y}d\alpha} \tag{5}$$

$$k_a = \sum_{i=1}^{N} \frac{1}{\int_{-\alpha_1}^{\alpha_2} \frac{(\alpha_2 - \alpha)\cos\alpha \sin^2\alpha_1}{2E[\sin\alpha + (\alpha_2 - \alpha)\cos\alpha]\Delta y} d\alpha} \tag{6}$$

$$\frac{1}{k_f} = \frac{\cos^2\alpha_1}{EB}\left[L^*\left(\frac{u_f}{S_f}\right)^2 + M^*\left(\frac{u_f}{S_f}\right) + P^*(1+Q^*\tan^2\alpha_1)\right] \tag{7}$$

where U_h, U_b, U_s, and U_a denote the Hertzian contact, bending, shear, and axial-compression strain energies of the gear pair, respectively; F is the meshing force along the meshing line; E, G, and V correspond to the elastic modulus, shear modulus, and Poisson's ratio, respectively; B refers to the tooth width, and I_x denotes the moment of inertia of the cross-section at the reference circle x of the gear; A_x is the cross-sectional area; d denotes the distance from the contact point to the base circle measured along the tooth-height direction; h denotes the distance from the mesh point to the gear centre; α_1 is the angle between the meshing force F and the direction perpendicular to the gear center; N represents the number of slices for helical gears; $\Delta y = l/N$; l denotes the projection of the contact-line length onto the face-width direction; α_1' denotes the angle of the mesh force at the slice contact point, measured relative to the direction normal to the gear axis. The matrix stiffness k_f includes parameters u_f and S_f[34].

$$u_f = r_b[(\alpha_1 + \alpha_2)\sin\alpha_1 + \cos\alpha_1] - r_f \tag{8}$$

$$S_f = 2r_f\theta_f \tag{9}$$

Regarding the polynomial representations of L^*, M^*, P^*, and Q^* [35]:

$$X_i^*(h_{fi}, \theta_f) = A_i/\theta_f^2 + B_i h_{fi}^2 + C_i h_{fi}/\theta_f + D_i/\theta_f + E_i h_{fi} + F_i \tag{10}$$

where X_i^* represents coefficients L^*, M^*, P^*, and Q^*; $h_{fi} = r_f/r_{int}$; r_{int} and θ_f as shown in Fig. 6; The values of A_i, B_i, C_i, D_i, E_i, and F_i are as shown in the table below.

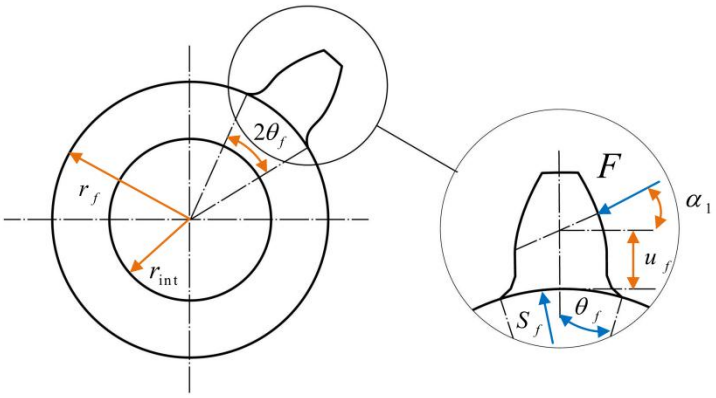


Fig. 6. Geometric parameters of gear wheel deformation.

Table 1.

Coefficients for wheel body-related formulas.

	$L^*(h_{fi},\theta_f)$	$M^*(h_{fi},\theta_f)$	$P^*(h_{fi},\theta_f)$	$Q^*(h_{fi},\theta_f)$
A_i	-5.574×10^{-5}	60.11×10^{-5}	-50.952×10^{-5}	-6.2042×10^{-5}
B_i	-1.9986×10^{-3}	28.100×10^{-3}	185.50×10^{-3}	9.0889×10^{-3}
C_i	-2.3015×10^{-4}	-83.431×10^{-4}	0.0538×10^{-4}	-4.0964×10^{-4}
D_i	4.7702×10^{-3}	-9.9256×10^{-3}	53.300×10^{-3}	7.8297×10^{-3}
E_i	0.0271	0.1624	0.2898	-0.1472
F_i	6.8045	0.9086	0.9236	0.6904

In summary, a parallel combination of slice-wise stiffness contributions over the face width yields the equivalent mesh stiffness of the helical gear pair, expressed as:

$$k=\frac{1}{\frac{1}{\mathrm{k_h}}+\frac{1}{k_{b1}}+\frac{1}{k_{s1}}+\frac{1}{k_{a1}}+\frac{1}{\mathrm{k_{f1}}}+\frac{1}{k_{b2}}+\frac{1}{k_{s2}}+\frac{1}{k_{a2}}+\frac{1}{\mathrm{k_{f2}}}} \tag{11}$$

where K_h, K_b, K_s, K_a, and K_f denote the Hertzian contact stiffness, tooth-root bending stiffness, shear stiffness, axial-compression stiffness, and foundation-compliance stiffness, respectively, and subscripts 1 and 2 refer to the driving and driven gears.

2.2. Random Speed Simulation

In practical applications, gear rotational speed is subject to multiple sources of uncertainty and often exhibits random fluctuations. Such random speed variation is not restricted to a particular operating scenario but is commonly encountered across a wide range of mechanical transmission systems. This motivates the development of a general analysis framework to quantify the effects of random speed excitation on the dynamic behaviour of geared transmissions.

To capture the time-varying characteristics of the random rotational speed, the K-L expansion is employed in this study for modelling and numerical simulation of the random speed process. The K－L expansion represents the random speed process as a finite set of mutually independent random variables and deterministic temporal basis functions, It achieves the minimum mean-square error for a given number of expansion terms [36], thereby providing a high-accuracy representation of non-stationary random excitations. The random rotational speed process $\dot{\theta}(t)$ of a gear system can be modelled as a Gaussian stochastic process. Its mean function $\dot{\theta}_m$ and variance function $\delta(t)$ can be determined accordingly. The random speed process is then decomposed using the K-L expansion as follows:

$$\dot{\theta}(t)=\dot{\theta}_{\mathrm{m}}+\dot{\theta}^{\mathrm{D}}(t)=\dot{\theta}_{\mathrm{m}}+\sum_{\mathrm{i=1}}^{\mathrm{M}}\sqrt{\lambda_i}\varphi_i(t)\xi_i \tag{12}$$

where $\theta(t)$ represents a standard Gaussian random field; t represents the point coordinate in a one-dimensional space within a random discrete velocity domain; M is the truncation order of the expansion; λ_i and $\varphi_i(t)$ represent the i-th eigenvalue and eigenvector of the autocorrelation function, respectively; ξ_i is a random variable of the velocity field.

Gear rotational speed is modelled as a stochastic process in the simulations. The accuracy of the results is mainly influenced by the autocovariance function and the truncation level of the K-L representation. In general, increasing the number of expansion terms improves approximation accuracy relative to the original stochastic process; however, an excessive number of terms can lead to substantially higher computational complexity and reduced numerical efficiency. To this end, the expansion accuracy error is introduced in this study as an evaluation metric to quantify the approximation performance of the finite-term K−L expansion with respect to the original stochastic process. This error is defined as follows:

$$\delta=\left|1-\frac{\tilde{z}_{ij}}{z_{ij}}\right| \tag{13}$$

where δ represents the random error in seed selection; $\tilde{z}_{ij}$ denotes the covariance value at position i, j after K-L expansion; z_{ij} denotes the covariance value of the original data at positions i, j.
Where the squared-exponential kernel is used as the covariance kernel for the random rotational speed process. Its mathematical expression is given as follows:

$$f\left(t_1,t_2\right)=\delta^2\times e^{-\frac{\left(t_1-t_2\right)^2}{\mathrm{L_c}^2}} \tag{14}$$

Using the K-L expansion, the continuous random rotational speed process can be discretised into a set of statistically representative random samples, each representing a distinct realisation of the stochastic speed trajectory. To quantitatively characterise the dispersion of these samples with respect to the population mean, the coefficient of variation is introduced as a statistical measure, defined as follows:

$$CV=\frac{\delta(t)}{\dot{\theta}_{\mathrm{m}}} \tag{15}$$

2.3. Time-domain Formulation of Meshing Stiffness

The meshing process for a single helical tooth can be conceptually divided into three primary phases: single-tooth, multi-tooth, and transitional. As illustrated in Fig. 9, a complete meshing cycle of a helical gear tooth can be further subdivided into four distinct sub-phases, namely single-tooth meshing, engaging transition, multi-tooth meshing, and disengaging transition.

The peak mesh stiffness can be estimated from the mean stiffness of all engaged tooth pairs during the multi-pair contact phase.

$$\mathrm{k_{double}}=\frac{\int_{\theta_1}^{\theta_2}k(\theta)d\theta}{\theta_2\text{-}\theta_1} \tag{16}$$

The minimum mesh stiffness is estimated as the mean stiffness of the engaged tooth pair during the single-pair contact phase.

$$\mathrm{k_{single}}=\frac{\int_{\theta_3}^{\theta_4}k(\theta)d\theta}{\theta_4\text{-}\theta_3} \tag{17}$$

For helical gear meshing, the maximum and minimum stiffness values can be treated as constants. During the mesh-in and mesh-out transitions, the mesh stiffness varies continuously with the contact position and is approximated using a linear interpolation.

During the engagement transition, the mesh stiffness is approximated by a linear segment with slope k_1:

$$\mathrm{k_1}=\frac{\mathrm{k_{double}}\text{-}\mathrm{k_{single}}}{\theta_1\text{-}\mathrm{O}} \tag{18}$$

Immediately after engaging the transition section, the meshing stiffness function is k_+:

$$k_+=\mathrm{k_1}\times\theta+\mathrm{k_{single}} \tag{19}$$

During the disengagement transition, the mesh stiffness is approximated by a linear segment with slope k_2:

$$\mathrm{k_2}=\frac{\mathrm{k_{single}}\text{-}\mathrm{k_{double}}}{\theta_3\text{-}\theta_2} \tag{20}$$

Immediately after the end of the engagement transition section, the mesh stiffness function is k_-:

$$k_-=\mathrm{k_2}\times\theta+\mathrm{k_{double}} \tag{21}$$

The equivalent stiffness in the spatial domain is denoted as k:

$$k=\begin{cases} k_{+}\theta+k_{\sin gle} & \theta\in[0,\theta_1] \\ k_{double} & \theta\in[\theta_1,\theta_2] \\ k_{-}\theta+k_{double} & \theta\in[\theta_2,\theta_3] \\ k_{\sin gle} & \theta\in[\theta_3,\theta_4] \end{cases} \tag{22}$$

The relationship between rotational speed and angular displacement enables the transformation of meshing stiffness into the time domain.

$$k=\begin{cases} k_{+}t+k_{\sin gle} & t\in[0,\mathrm{T}_1] \\ k_{double} & t\in[T_1,T_2] \\ k_{-}t+k_{double} & t\in[T_2,T_3] \\ k_{\sin gle} & t\in[T_3,T_4] \end{cases} \tag{23}$$

where T_1, T_2, T_3, and T_4 denote the times corresponding to the meshing intervals, $T_h=60\times\frac{\theta_h-\theta_{h-1}}{n}$.q takes the discrete values 1, 2, 3, and 4, while n denotes the rotational speed.

2.4. Nonlinear Dynamic System of Helical Gears

As illustrated in Fig. 7, a nonlinear dynamic model with bending–torsional–axial coupling is constructed for a helical gear pair subjected to random rotational-speed excitation to analyse its meshing dynamics [37]. A six-DOF dynamic model is formulated to capture the relative vibration and nonlinear response of the gear pair.

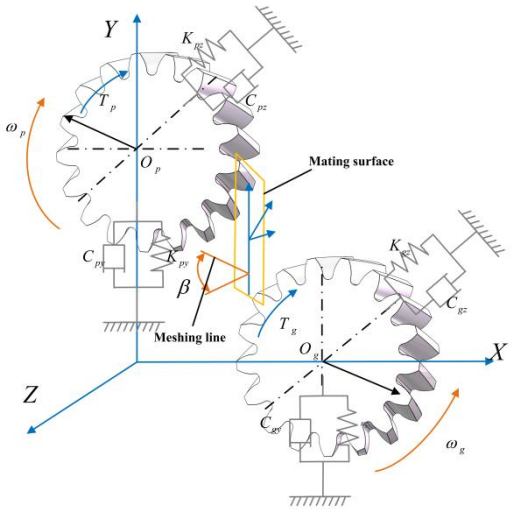


Fig. 7. Dynamic model of helical gear pair.

where R denotes the pitch radius, T represents the transmitted torque, and ω indicates the angular velocity of the gear. To formulate the governing equations, a set of generalised coordinates is defined to represent the translational and torsional motions of the gear pair:

$$\{X\}=\begin{Bmatrix} y_p & y_g & z_p & z_g & \theta_p & \theta_g \end{Bmatrix} \tag{24}$$

where y, z, and θ denote the radial displacement, axial displacement, and angular displacement of the meshing point of the helical gears, respectively, At the same time, p and g refer to the driving and driven gears, respectively. Assuming the active helical gear has a right-hand thread and a helix angle of β, the relationship between radial displacement and axial displacement at the point of contact can be derived as follows:

$$z = y\tan\beta \tag{25}$$

The displacement at the mesh point P is related to the driving-gear generalised coordinates, and can be written as:

$$\tilde{y}_p = y_p + \theta_p \mathrm{R_p} \tag{26}$$

$$\tilde{z}_p = z_p - \tilde{y}_p \tan\beta = z_p - (y_p + \theta_p \mathrm{R_p})\tan\beta \tag{27}$$

where $\tilde{\mathrm{y}}_\mathrm{p}$ and $\tilde{\mathrm{z}}_\mathrm{p}$ denote the actual vibration displacement at the meshing point *P*. The displacement at the mesh point G and the driven-gear generalized coordinates are written as:

$$\tilde{y}_g = y_g - \theta_g \mathrm{R_g} \tag{28}$$

$$\tilde{z}_g = z_g - \tilde{y}_g \tan\beta = z_g - (y_g - \theta_g \mathrm{R_p})\tan\beta \tag{29}$$

where $\tilde{y}_g$ and $\tilde{z}_g$ represent the actual vibration displacement at the meshing point *G*.

In the simplified helical gear dynamics model, the normal stiffness is set to *K*, the normal damping to c_f, the normal meshing error to e, and the normal flank clearance to 2b. The axial and lateral stiffness, damping, clearance, and error are assumed to be equal constant values. During the gear meshing process, the backlash is assumed to be symmetric, and the corresponding clearance function can be expressed as:

$$f(q) = \begin{cases} q - \mathrm{b} & q > \mathrm{b} \\ 0 & -\mathrm{b} \le q \le \mathrm{b} \\ q + \mathrm{b} & q < -\mathrm{b} \end{cases} \tag{30}$$

During gear meshing, contact between the tooth surfaces generates dynamic meshing force components in both the tangential and axial directions. The tangential dynamic mesh force can be written as:

$$\begin{aligned} F_y &= k_y f_y(\tilde{y}_p - \tilde{y}_g - \mathrm{e_y}) + \mathrm{c_y}(\dot{\tilde{y}}_p - \dot{\tilde{y}}_g - \dot{e}_y) \\ &= \cos\beta[k_f f_y(y_p + \theta_p \mathrm{R_p} - (y_g - \theta_g \mathrm{R_g}) - \mathrm{e_y}) \\ &\quad + \mathrm{c_f}(\dot{y}_p + \dot{\theta}_p \mathrm{R_p} - (\dot{y}_g - \dot{\theta}_g \mathrm{R_g}) - \dot{e}_y)] \end{aligned} \tag{31}$$

The axial dynamic meshing force can be expressed as:

$$\begin{aligned} F_z &= k_z f_z(\dot{z}_p - \dot{z}_g - \mathrm{e_z}) + \mathrm{c_y}(\dot{z}_p - \dot{z}_g - \dot{e}_z) \\ &= \sin\beta\{k_f f_z[z_p - (y_p + \theta_p \mathrm{R_p})tan\beta - (z_g - (y_g - \theta_g \mathrm{R_p})\tan\beta) - \mathrm{e_z}] \\ &\quad + \mathrm{c_f}[\dot{z}_p - (\dot{y}_p + \dot{\theta}_p \mathrm{R_p})\tan\beta - (\dot{z}_g - (\dot{y}_g - \dot{\theta}_g \mathrm{R_g})\tan\beta) - \dot{e}_z]\} \end{aligned} \tag{32}$$

Dynamic analysis based on simplified models and force analysis:

$$
\begin{aligned}
\mathrm{m_p}\,\ddot{y}_p + \mathrm{c_y}\dot{y}_p + k_y f_y(y_p) &= -F_y \\
\mathrm{m_g}\,\ddot{y}_g + \mathrm{c_y}\dot{y}_g + k_y f_y(y_g) &= F_y \\
\mathrm{m_p}\,\ddot{z}_p + \mathrm{c_z}\dot{z}_p + k_z f_z(z_p) &= F_z \\
\mathrm{m_g}\,\ddot{z}_g + \mathrm{c_z}\dot{z}_g + k_z f_z(z_g) &= -F_z \\
\mathrm{I_p}\,\ddot{\theta}_p &= \mathrm{T_p} - F_y \mathrm{R_p} \\
\mathrm{I_g}\,\ddot{\theta}_g &= -\mathrm{T_g} + F_y \mathrm{R_g}
\end{aligned}
\tag{33}
$$

In the context of dynamic analysis, this paper focuses on dynamic analysis under different rotational speed conditions. For the study, parameters such as load torque, driving torque, and static error are treated as constants, thereby simplifying the analysis.

This study investigates the dynamic behaviour of the helical gear system subjected to random rotational-speed excitation. To reduce computational complexity and emphasise the influence of speed variations on the system's dynamic behaviour, the parameters-load torque, driving torque, and static transmission error-are treated as constants throughout the analysis.

Overall, the proposed nonlinear dynamic model with bending–torsional–axial coupling effectively captures the system's time-varying behaviour under stochastic rotational-speed excitation. To facilitate numerical computation and subsequent dynamic response analysis, the parameters of the helical gear pair listed in Table 2 are adopted as the model input conditions.

Table 2

Gear parameters.

Parameters	Driving wheel	Driven wheel
Number of teeth z	17	44
Gear rotation direction	Left	Right
Normal module (mm)	6	
Normal pressure angle α/(°)	20	
Helix angle β/(°)	24.43	
Torque T/(N·m)	193.2	500
Modulus of elasticity (E/GPa)	210	

3. Results

3.1. Meshing Stiffness Calculation and Time-Domain Transformation

A coupled slicing discretisation and energy-based formulation is adopted to obtain the helical-gear mesh-stiffness evolution, after which a simplified stiffness profile is constructed for dynamic analysis. As shown in Fig. 8(a), the entire meshing process can be divided into three stages: the single-pair, double-pair, and transition contact regions. The simplified time-domain stiffness function facilitates a more intuitive analysis of how the system dynamics vary under different random speed processes.[38]

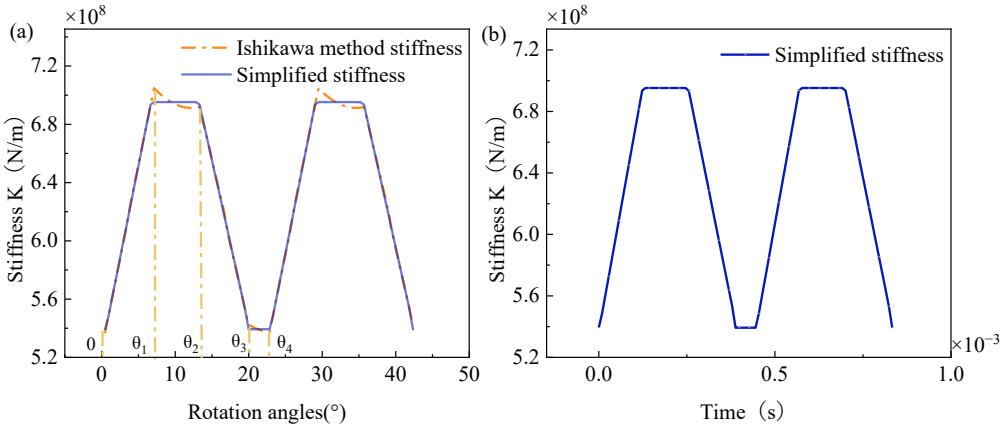


Fig. 8. Stiffness simplification and transformation.

3.2. Dynamic Analysis of Different Random Samples at the Same Relevant Length

A K-L representation is adopted to model the stochastic rotational-speed process. Based on this representation, the effects of random speed excitation on the system dynamics are analysed, and the corresponding TVMS is evaluated.

Taking the random rotational speed with an autocorrelation length of L_c=0.25 as an example, the 2000th, 5000th, and 8000th samples of the random process are selected as inputs to obtain the variations in meshing stiffness under different random excitations. Fig. 9(a-c)respectively, present the time-varying rotational speed (red) and the corresponding TVMS (black) for three sets of random speed samples. From the three sets of rotational speed and stiffness variation curves, it can be observed that although the random rotational speeds differ in initial values and fluctuation amplitudes, all three sets of time-varying meshing stiffness exhibit the same variation trend. The characteristic time scale of meshing-stiffness variation decreases with increasing rotational speed. Moreover, as the amplitude of rotational-speed fluctuations increases, the meshing stiffness exhibits more pronounced time-varying fluctuations.

For each random-speed realisation, the associated time-dependent mesh-stiffness history is prescribed in the dynamic model to obtain the system response. Fig. 9(a) shows the analysis results for the 2000th random rotational speed sample with an autocorrelation length L_c = 0.25, including the radial time-domain response (blue line). It can be observed that, within the initial 0-1s interval, the rotational speed exhibits a random fluctuation process, featuring a gradual increase followed by a rapid decrease. The radial response contains both high-frequency components induced by the meshing stiffness and low-frequency components associated with the rotational speed fluctuations. Fig. 9(b-c) show the dynamic responses corresponding to the 5000th and 8000th random samples, respectively. In comparison with the 2000th sample, all three samples exhibit distinct patterns and amplitudes of rotational speed fluctuations. Nevertheless, the periodic variations in meshing stiffness and the overall trends of the radial responses remain consistent. These observations collectively demonstrate that random fluctuations in rotational speed can degrade the system's transient stability. Fig. 9(e-f) present the axial time-domain responses of the 2000th, 5000th, and 8000th random samples, respectively. The results show that the amplitude of axial displacement fluctuations is strongly correlated with the variations in rotational speed. As the average rotational speed increases, the magnitude of the initial meshing impacts becomes significantly larger. In the subsequent stage, higher instantaneous speeds enable the system to enter a vibration regime governed by random fluctuations more rapidly. A comparative examination of the rotational speed fluctuation patterns and the corresponding axial displacement responses further indicates that acceleration–deceleration sequences lead to more pronounced axial vibration than deceleration–acceleration sequences. In summary, across different random-speed realisations, the response components in the radial and axial directions exhibit pronounced non-stationary fluctuations.

The radial and axial response spectra are evaluated using the Fast Fourier Transform (FFT). Fig. 10 presents the corresponding radial and axial amplitude-frequency characteristics for the 2000th, 5000th, and 8000th random samples.

Fig. 10(a) illustrates the frequency-domain characteristics in the radial direction. It can be seen that the radial vibration amplitude is significantly higher than that in the axial direction, and the dominant

peak frequency varies with the stochastic rotational speed. For the 2000th sample, the dominant radial peak occurs at approximately 150-230 Hz, with a peak amplitude of about 1.25×10^{-5}. When the 5000th sample is considered, the dominant peak frequency moves to 180-260 Hz as the rotational speed increases, and the corresponding peak amplitude rises to 1.65×10^{-5}. For the 8000th sample, the dominant peak continues to drift toward the 200-300 Hz range, reaching a peak amplitude of 1.95×10^{-5}. This continuous drift of the dominant peak with changes in the random rotational speed indicates that, under random excitation, the radial vibration meshing frequency exhibits pronounced dynamic instability. Fig. 10(b) presents the frequency-domain response in the axial direction. The axial vibration energy is likewise mainly concentrated within the 0-300 Hz range, corresponding to the meshing frequency and its related natural frequency components. For the 2000th sample, the dominant axial energy lies between 150 and 250 Hz, with a peak amplitude of approximately 0.22×10^{-6}. When the number of samples increases to 5000, the dominant frequency shifts slightly upward to 180-280 Hz, and the peak amplitude increases to 0.28×10^{-6}. For the 8000th sample, the dominant peak further moves to the 200-300 Hz range, with a peak amplitude of about 0.32×10^{-6}. Although the axial vibration amplitude is generally smaller and its spectral distribution smoother than in the radial direction, its dominant peak frequency also exhibits a persistent drift as the random rotational speed varies. This demonstrates that both axial and radial vibrations exhibit clear time-varying behaviour, and that the system's vibration stability degrades noticeably under random rotational-speed excitation.

A comprehensive analysis of the radial and axial frequency-domain responses indicates that, under random rotational speed excitation, the system’s meshing frequency varies with the instantaneous rotational speed. In contrast, the radial vibration amplitude is markedly greater than that in the axial direction. Both spectra exhibit meshing-frequency drift and amplitude fluctuations associated with speed variations, indicating a degree of meshing instability under random rotational speeds.

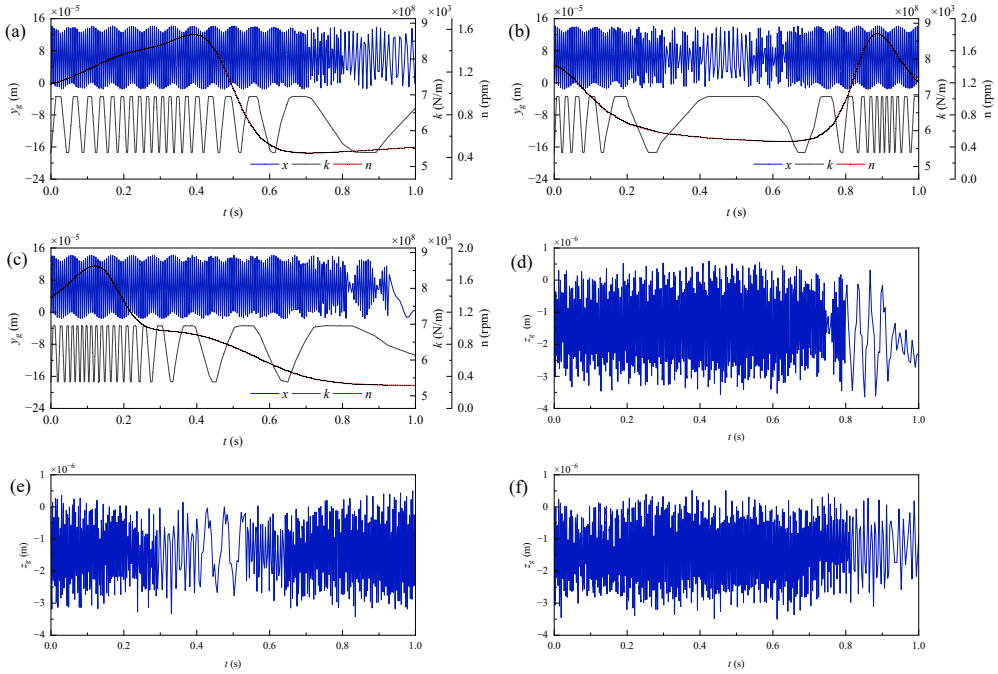


Fig. 9. Time-domain analysis.

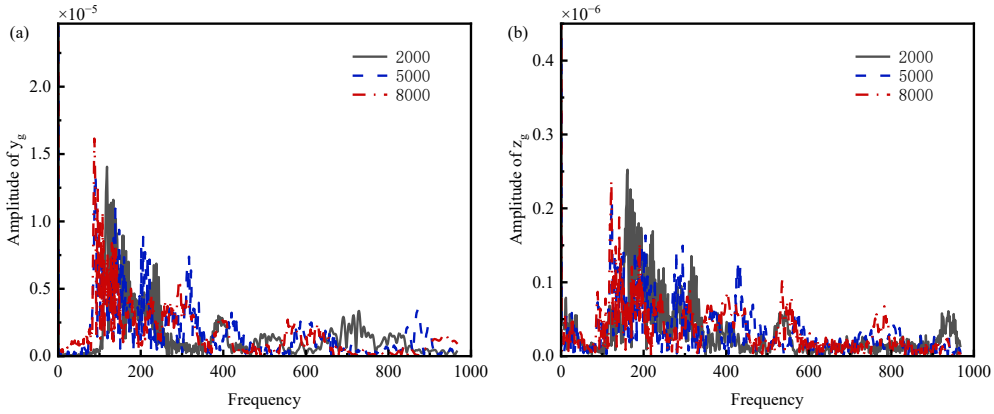


Fig. 10. Frequency domain analysis.

3.3. Statistical Analysis of Dynamics in Single-Correlation-Length Random Processes

When subjected to random rotational-speed excitation, the helical gear system response becomes highly stochastic and nondeterministic, and therefore cannot be accurately captured by conventional deterministic approaches. To uncover the statistical patterns governing the system response under such stochastic speed excitation, statistical feature analysis is employed to investigate its dynamic behaviour.

A statistical analysis of the radial and axial dynamic responses of the helical gear system is performed under a random rotational speed process with a correlation length L_c=0.25. Fig. 11 presents the statistical results in the radial direction, where y_g represents the radial displacement and $\dot{y}_g$ denotes the radial velocity. As shown in Fig. 11(a), the mean radial displacement E[y_g] experiences an impact at the onset of meshing. Subsequently, due to damping, the oscillation amplitude gradually decreases and eventually fluctuates randomly around approximately 6.35×10−5m. As shown in Fig. 11(b) illustrates the mean radial velocity $E(\dot{y}_g)$, which fluctuates randomly around zero, indicating pronounced velocity randomness during the meshing process. Fig. 11(c) illustrates the variation trend of the radial displacement variance Var[y_g]. The variance increases rapidly during the initial stage, then decays, and eventually fluctuates randomly around approximately 2.58×10^{-9}. This behaviour indicates that, in the later stages of meshing, the gear's radial displacement primarily undergoes random oscillations around its mean value. Fig. 11(d) shows the covariance $\mathrm{Cov}[y_g, \dot{y}_g]$ between the radial displacement and velocity. It exhibits large fluctuation amplitudes during the initial meshing stage, followed by a gradual attenuation toward zero, indicating that the correlation between displacement and velocity weakens progressively over time. Overall, the helical gear system exhibits some degree of disturbance resistance under random rotational-speed excitation. The relatively low mean and variance indicate that the radial meshing response remains generally stable. At the same time, the gradual reduction in covariance suggests a progressive weakening of the coupling between displacement and velocity, helping mitigate potential resonance risks.

Fig. 12 presents the statistical results for the axial response of the helical-gear system with correlation length L_c=0.25, where z_g represents the axial displacement and $\dot{z}_g$ denotes the axial velocity. Fig. 12(a) shows that the mean axial displacement E[z_g] experiences a pronounced impact during the initial meshing stage and further increases as double-tooth engagement develops. Due to damping, the displacement gradually stabilises around -1.44×10^{-6}m, with random fluctuations thereafter. Fig. 12(b) shows the mean axial velocity E[Y]. During the initial meshing stage, it experiences a pronounced impact. As the alternating single-tooth and double-tooth engagements are established, the velocity rises instantaneously and then gradually approaches zero, exhibiting random fluctuations. This behaviour indicates that a complete alternating-mesh characteristic forms within the nodal region of the system. Fig. 12(c) shows the variance of axial displacement Var[z_g]. The variance increases rapidly during the initial stage due to meshing effects, then decreases markedly under the combined effects of damping and alternating meshing. This behaviour indicates that the system has a strong ability to suppress axial fluctuations. Fig. 12(d) shows the covariance $\mathrm{Cov}[z_g, \dot{z}_g]$ between the axial displacement and velocity. It exhibits pronounced fluctuations during the initial meshing stage, followed by rapid decay and random oscillations around zero, indicating a relatively weak correlation between axial displacement

and velocity. The combined statistical analysis of the radial and axial directions reveals that the helical gear system exhibits pronounced directional differences in its dynamic response under random rotational speed conditions. The radial response is more sensitive to random excitation, whereas the axial response demonstrates stronger disturbance resistance. The lower variance and the rapid attenuation of covariance in the axial direction indicate that the system experiences smaller response amplitudes to random disturbances along this direction, thereby exhibiting superior resistance to stochastic excitation.

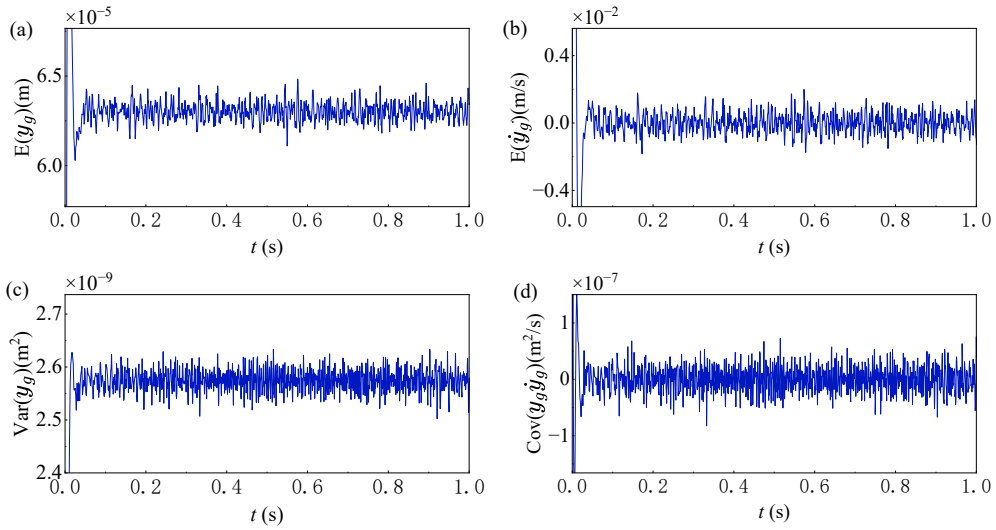


Fig. 11. Analysis of radial random process response with a correlation length of 0.25.

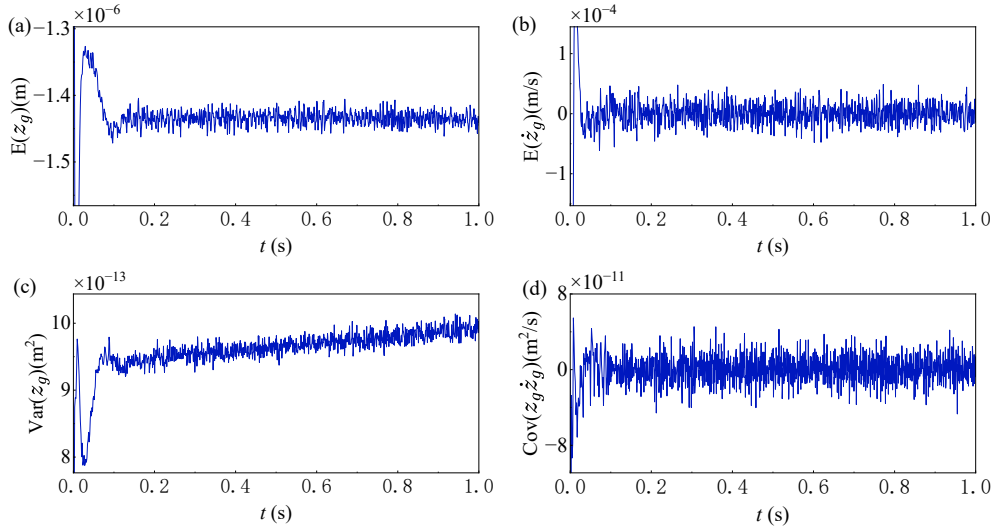


Fig. 12. Response analysis of axial random process with a relevant length of 0.25.

3.4. Analysis of Statistical Properties at Different Engagement Times in Stochastic Processes

To examine the displacement distribution characteristics of the helical gear system under varying random rotational speeds, a correlation length of L_c=0.25 was adopted, and the random speed process was discretised into 1936 time points. On this basis, the displacement probability distribution histograms corresponding to the 500th, 1000th, and 1500th time points were extracted for analysis. In addition, the first four statistical moments and the coefficient of variation of both radial and axial displacements were computed, and the results are summarised in Table 3.

Fig. 13 shows the histograms of the radial and axial displacements of the helical gear at three time instants (500, 1000, and 1500). The radial displacement exhibits a precise bimodal distribution at all time points, with well-defined and highly symmetric peaks. The distribution centre remains

consistently around 5.8 × 10^{-5} m, and s summarised in Table 3, the standard deviation of the radial displacement is on the order of 10^{-5}, indicating relatively small fluctuation amplitudes. The skewness is close to zero, which is consistent with the symmetric bimodal pattern observed in Fig. 13. The kurtosis is around 1.5, lower than that of a standard normal distribution, implying a flatter distribution. This indicates that the radial-displacement fluctuations are predominantly clustered around the mean value, highlighting the role of time-varying mesh stiffness in shaping the radial response. In contrast, the axial displacement does not exhibit a pronounced unimodal distribution. Instead, it shows only a weakly bimodal structure, with substantially lower peakedness than that observed in the radial direction. The corresponding peak count is roughly 260. According to Table 3, the mean axial displacement is about -1.42×10^{-6} m, and its standard deviation is on the order of 10^{-6} , n order of magnitude smaller than that of the radial displacement-indicating much weaker random fluctuations in the axial direction. The skewness oscillates slightly around zero, suggesting a nearly symmetric distribution. As time progresses, the kurtosis of the axial displacement gradually increases, indicating that the distribution spreads across a wider interval.

In summary, the statistical characteristics of the displacement responses in the helical gear system under random rotational speed excitation exhibit pronounced differences between the radial and axial directions. The radial displacement is strongly influenced by the time-varying meshing stiffness, exhibiting a distinct, clearly bimodal nonlinear distribution. In contrast, the axial displacement shows only a weak bimodal pattern, and its statistical behaviour is closer to a low-peaked, non-Gaussian distribution, indicating that random speed fluctuations exert a relatively minor effect on the axial meshing response.

Table 3

First four moments and coefficients of variation for radial and axial displacements at different time instants.

Time	Direction	Mean(m)	Standard deviation(m)	Skewness	kurtosis	CV(%)
1	y_g	6.35×10^{-5}	5.06×10^{-5}	-0.0165	1.5425	79.5985
	z_g	-1.42×10^{-6}	9.77×10^{-7}	-0.0356	1.9610	65.8856
2	y_g	6.25×10^{-5}	5.07×10^{-5}	0.0114	1.5287	81.1304
	z_g	-1.42×10^{-6}	9.89×10^{-7}	-0.0283	1.9917	67.2779
3	y_g	6.25×10^{-5}	5.13×10^{-5}	0.0098	1.5109	81.9806
	z_g	-1.45×10^{-6}	1.01×10^{-6}	0.0126	2.0787	69.5022

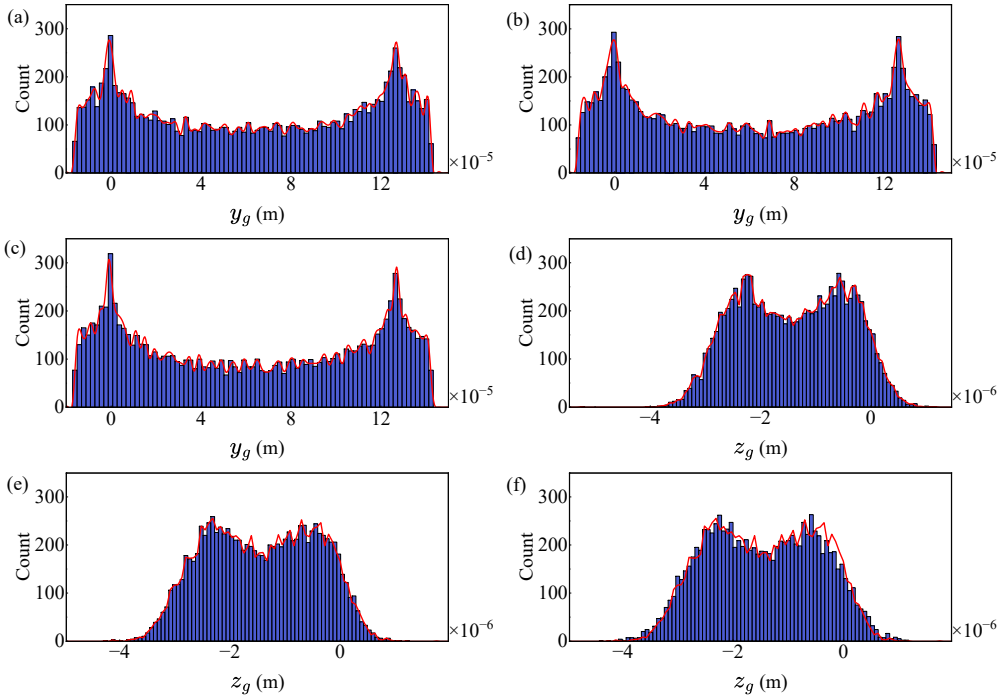


Fig. 13. Histogram of axial displacement at different time instants.

3.5. Dynamic Characteristics Analysis at Different Random Velocities

To examine how the autocorrelation length of random rotational-speed excitation affects the helical gear system response, three operating cases are considered (Lc=0.25, 0.35, and 0.45). Using the Monte Carlo method, 10,000 random samples are generated and analyzed via dynamic numerical simulations.

Fig. 14 illustrates the time-domain statistical characteristics in radial displacement, radial velocity, variance, and covariance of the helical gear system under different autocorrelation lengths. As shown in Fig. 14(a), the fluctuation intensity of the radial vibration shows a progressive reduction as the autocorrelation length increases from 0.25 to 0.45, with the slightest fluctuation observed at L_c=0.45. As shown in Fig. 14(b), the fluctuation amplitude of the radial velocity decreases with increasing autocorrelation coefficient, indicating that the fluctuation amplitude of the input random rotational speed is positively correlated with the amplitude of the random response in radial velocity.As shown in Fig. 14(c), the variance of the system's output displacement gradually increases as the autocorrelation coefficient of the input random rotational speed decreases. The variance reaches its maximum at L_c=0.25 and its minimum at L_c=0.45. As shown in Fig. 14(d), random rotational speeds with smaller autocorrelation coefficients exert a weaker influence on the covariance values. With increasing autocorrelation coefficient, the covariance between radial displacement and radial velocity appears later in time, while its peak value becomes higher than that corresponding to smaller autocorrelation coefficients. Fig. 15 presents the temporal evolution of the axial displacement and velocity, along with their associated statistical quantities, for the helical gear system under different correlation lengths. It can be observed that the axial response follows the same general trend as the radial response. In the initial stage, a distinct transient response emerges due to the applied input disturbance. Subsequently, due to damping, the statistical quantities enter a regime of relatively smooth random fluctuations, whose amplitudes gradually decrease as the correlation length increases.

Combined statistical analyses of both radial and axial responses show that, as speed autocorrelation increases, the radial response and its variance show a slight overall reduction, whereas the axial variance decreases more noticeably. Meanwhile, the displacement – velocity covariance in both directions exhibits a delayed, amplified peak: the peak occurs later and becomes larger as the autocorrelation increases, indicating enhanced statistical coupling in the system response.

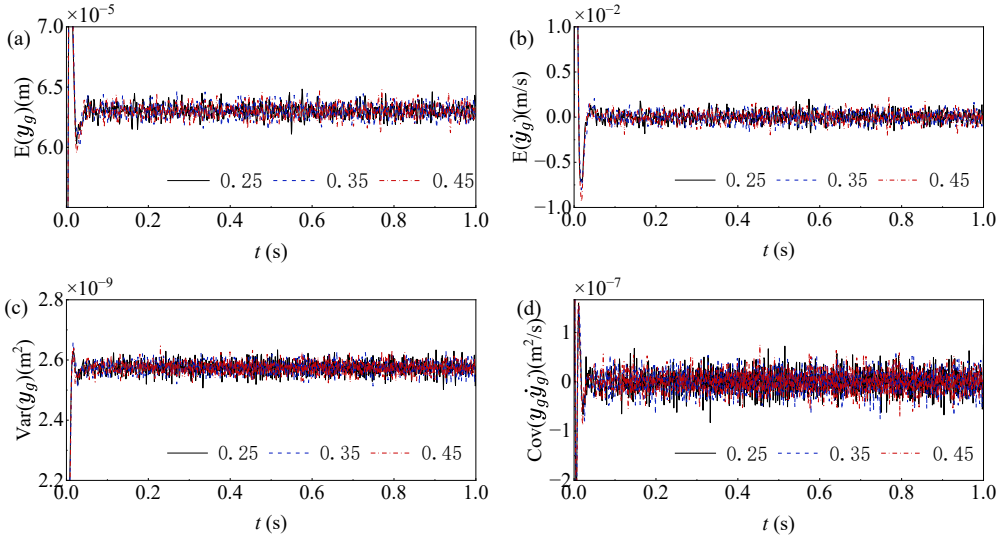


Fig. 14. Radial time domain for different correlation lengths.

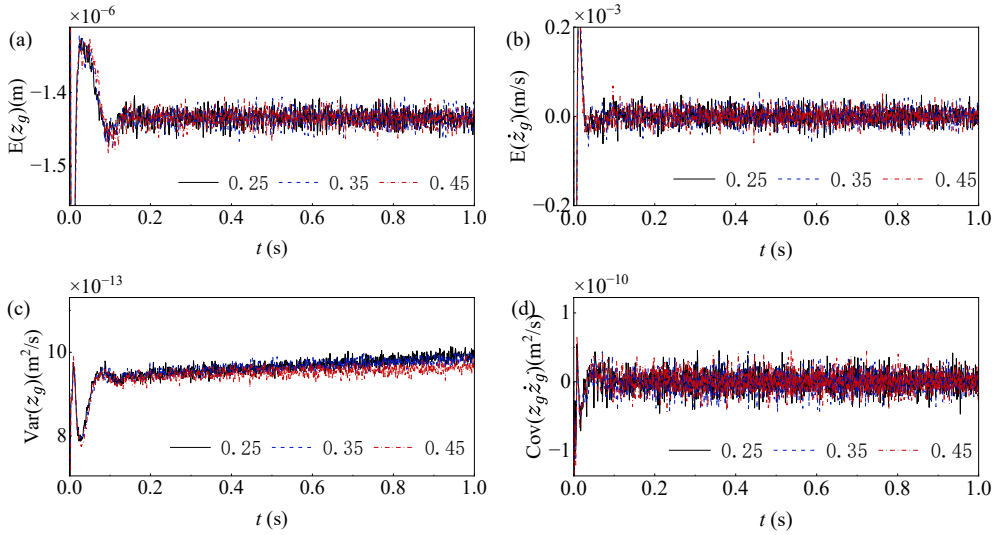


Fig. 15. Axial time domain for different correlation lengths.

4. Conclusion

This study investigates the nonstationary vibration response of a helical gear pair under random speed excitation. A random-speed modeling approach is presented; the associated time-varying meshing stiffness is derived and simplified; and the response statistics are analyzed using a nonlinear dynamic model with coupled bending, torsional, and axial motions. The main findings are summarized as follows:

- For a given autocorrelation length, the radial displacement is generally larger than the axial displacement, and the axial response exhibits smoother time-domain fluctuations. Statistical results based on 10,000 random speed realizations show that the axial response has a much smaller dispersion than the radial response, indicating a more concentrated variation range. The displacement distributions in both directions are approximately symmetric, while the axial displacement is closer to a unimodal shape.
- The speed autocorrelation length modulates the statistical characteristics of the system response. For different autocorrelation lengths, the radial vibration amplitude consistently exceeds the axial one, and the radial response shows more pronounced fluctuations. In addition, no robust linear relationship is observed between the displacement response and the input speed. As the autocorrelation length increases, the displacement–velocity correlation strengthens in both radial and axial directions.

These findings indicate that random speed excitation not only changes the response amplitude but also alters the statistical dependence structure of the response. The proposed random process modeling and dynamic analysis approach can be applied to vibration assessment and parameter sensitivity analysis of gear transmissions operating under variable operating conditions, such as wind turbine drivetrains and automotive transmissions.

References

[1] S. Mo, W. Song, Y. Zhang, Y. Zhou, B. Yao, H. Houjoh and W. Zhang, A new iterative method for calculating the time-varying meshing stiffness of orthogonal face gear pairs, Mechanism and Machine Theory. 206 (2025) 105938, https://doi.org/10.1016/j.mechmachtheory.2025.105938.

[2] L. Zhen, L. Fucai, B. Wenjie and X. Xiaolei, Loaded tooth contact analysis and meshing stiffness calculation for cracked spiral bevel gears, Chinese Journal of Aeronautics. 38 (2025) 103085, https://doi.org/10.1016/j.cja.2024.05.041.

[3] G. Liu, L. Zhang, J. Liu, H. Li, G. Tong, P. Duan, H. Jiang, X. Kong and F. Liu, Dynamics analysis for an improved gear model considering velocity-dependent mesh stiffness with tooth root crack, Journal of Sound and Vibration. 600 (2025) 118872, https://doi.org/10.1016/j.jsv.2024.118872.

[4] Y. Wang, H. Wang, K. Li, B. Qiao, Z. Shen and X. Chen, An analytical method to calculate the time-varying mesh stiffness of spiral bevel gears with cracks, Mechanism and Machine Theory. 188 (2023) 105399, https://doi.org/10.1016/j.mechmachtheory.2023.105399.

[5] M. Feng, H. Ma, Z. Li, Q. Wang and B. Wen, An improved analytical method for calculating time-varying mesh stiffness of helical gears, Meccanica. 53 (2018) 1131 – 1145, https://doi.org/10.1007/s11012-017-0746-6.
[6] Q. Wang and Y. Zhang, A model for analyzing stiffness and stress in a helical gear pair with tooth profile errors, Journal of vibration and control. 23 (2017) 272 – 289, https://doi.org/10.1177/1077546315576828.
[7] X. Tang, L. Zou, W. Yang, Y. Huang and H. Wang, Novel mathematical modelling methods of comprehensive mesh stiffness for spur and helical gears, Applied Mathematical Modelling. 64 (2018) 524 – 540, https://doi.org/10.1016/j.apm.2018.08.003.
[8] F. Liu, Y. Chen, H. Xie, B. Lu and B. Chen, Study on the meshing stiffness of plastic helical gear meshing with metal worm via point-contact, Mechanism and Machine Theory. 176 (2022) 105040, https://doi.org/10.1016/j.mechmachtheory.2022.105040.
[9] M. Rezaei, M. Poursina, S. H. Jazi and F. H. Aboutalebi, Calculation of time dependent mesh stiffness of helical planetary gear system using analytical approach, Journal of Mechanical Science and Technology. 32 (2018) 3537 – 3545, https://doi.org/10.1007/s12206-018-0704-9.
[10] W.-J. Chung, J.-H. Park, H.-G. Yoo, Y.-J. Park, S.-c. Kim, J. Sohn and G.-h. Lee, Improved analytical model for calculating mesh stiffness and transmission error of helical gears considering trochoidal root profile, Mechanism and Machine Theory. 163 (2021) 104386, https://doi.org/10.1016/j.mechmachtheory.2021.104386.
[11] C. Liu, W. Shi and K. Liu, Calculation method of mesh stiffness for helical gear pair with manufacturing errors, assembly errors and tooth modifications, Meccanica. 57 (2022) 541 – 565, https://doi.org/10.1007/s11012-022-01479-8.
[12] P. Marques, R. Martins and J. Seabra, Analytical load sharing and mesh stiffness model for spur/helical and internal/external gears – Towards constant mesh stiffness gear design, Mechanism and Machine Theory. 113 (2017) 126 – 140, https://doi.org/10.1016/j.mechmachtheory.2017.03.007.
[13] L. Wang, Y. Du, S. Dou, F. Liu, H. Bai, X. Jia , N. Li, Study on the meshing characteristics of helical gear pairs based on the improved potential energy method for meshing stiffness, Packaging Engineering. 46 (2025) 169 – 178, http://doi.org/10.19554/j.cnki.1001-3563.2025.03.020.
[14] Z. Wang, L. Shi, C. Chen, S. Yan , Z. Liu, Study on time-varying engagement stiffness calculation and inter-tooth load distribution for helical gears under tooth breakage conditions, Mechanical Strength. 45 (2023) 350 – 356, http://doi.org/10.16579/j.issn.1001.9669.2023.02.013.
[15] K. Huang, H. Wu, Calculation and analysis of time-varying engagement stiffness for spur gears based on an improved ishikawa method, Technology and Market. 30 (2023) 80 – 83.
[16] A.Kahraman and R. Singh, Non-linear dynamics of a spur gear pair, Journal of sound and vibration. 142 (1990) 49 – 75, https://doi.org/10.1016/0022-460X(90)90582-K.
[17] A. Kahraman and G. W. Blankenship, Interactions between commensurate parametric and forcing excitations in a system with clearance, Journal of Sound and Vibration. 194 (1996) 317 – 336, https://doi.org/10.1006/jsvi.1996.0361.
[18] G. Cheng, J. Ma, J. Li, K. Sun, K. Wang and Y. Wang, Study on the dynamic characteristics of gears considering surface topography in a mixed lubrication state, Lubricants. 12 (2023) 7, https://doi.org/10.3390/lubricants12010007.
[19] S. Wu, M. J. Zuo and A. Parey, Simulation of spur gear dynamics and estimation of fault growth, Journal of Sound and vibration. 317 (2008) 608 – 624, https://doi.org/10.1016/j.jsv.2008.03.038.
[20] Y. Yi, K. Huang, Y. Xiong and M. Sang, Nonlinear dynamic modelling and analysis for a spur gear system with time-varying pressure angle and gear backlash, Mechanical systems and signal processing. 132 (2019) 18 – 34, https://doi.org/10.1016/j.ymssp.2019.06.013.
[21] Z. Cao, Z. Chen and H. Jiang, Nonlinear dynamics of a spur gear pair with force-dependent mesh stiffness, Nonlinear Dynamics. 99 (2020) 1227 – 1241, https://doi.org/10.1007/s11071-019-05348-0.
[22] Y. Zhang, Q. Wang, H. Ma, J. Huang and C. Zhao, Dynamic analysis of three-dimensional helical geared rotor system with geometric eccentricity, Journal of Mechanical Science and Technology. 27 (2013) 3231 – 3242, https://doi.org/10.1007/s12206-013-0846-8.
[23] P. Velex and V. Cahouet, Experimental and numerical investigations on the influence of tooth friction in spur and helical gear dynamics, J. Mech. Des. 122 (2000) 515 – 522, https://doi.org/10.1115/1.1320821.
[24] C. Wang, S. R. Wang, B. Yang and G. Q. Wang, Dynamic modeling of double helical gears, Journal of Vibration and Control. 24 (2018) 3989 – 3999, https://doi.org/10.1177/1077546317717885.
[25] S. D. Yavuz, Z. B. Saribay and E. Cigeroglu, Nonlinear dynamic analysis of a drivetrain composed of spur, helical and spiral bevel gears, Nonlinear Dynamics. 100 (2020) 3145 – 3170, https://doi.org/10.1007/s11071-020-05666-8.
[26] H. Jiang, Y. Shao, C. K. Mechefske and X. Chen, The influence of mesh misalignment on the dynamic characteristics of helical gears including sliding friction, Journal of Mechanical Science and Technology. 29 (2015) 4563 – 4573, https://doi.org/10.1007/s12206-015-1001-5.
[27] P. Yan, H. Liu, P. Gao, X. Zhang, Z. Zhan and C. Zhang, Optimization of distributed axial dynamic modification based on the dynamic characteristics of a helical gear pair and a test verification, Mechanism and Machine Theory. 163 (2021) 104371, https://doi.org/10.1016/j.mechmachtheory.2021.104371.
[28] J. Chen, R. Zhu, W. Chen, M. Li, X. Yin and G. Dai, Nonlinear dynamic modeling and analysis of helical gear system with time-varying backlash caused by mixed modification, Nonlinear Dynamics. 111 (2023) 1193 – 1212, https://doi.org/10.1007/s11071-022-07872-y.
[29] M. Liu, Y. Qu, C. Hu and E. Deng, Lubrication performance of helical gear pair under dynamic load based on local involute profile, Journal of Tribology. 144 (2022) 021601, https://doi.org/10.1115/1.4050850.
[30] G. Mo, C. Liu, G. Liu and F. Liu, Improved nonlinear dynamic model of helical gears considering frictional excitation and fractal effects in Backlash, Machines. 13 (2025) 262, https://doi.org/10.3390/machines13040262.
[31] L. Liu, J. Ni, W. Jiang, Dynamic analysis of equal relative curvature gears considering time-varying effects, Mechanical transmission. 46 (2022) 10 – 15+69, http://doi.org/10.16578/j.issn.1004.2539.2022.11.002.
[32] L. Zhang, X. Wu, J. Xu, Y. zhang , Y.Zhang, Dynamic analysis of helical gears with time-varying meshing stiffness and pitch error, Mechanical transmission. 40 (2016) 149 – 154, http://doi.org/10.16578/j.issn.1004.2539.2016.06.033.

[33] W. Liu, R. Li, J. Zhang, T. Lin , Y. Yang , Research on modified algorithms for time-varying engagement stiffness of helical gears and influencing factors, Journal of Hunan university (natural science edition). 45 (2018) 1 – 10, http://doi.org/10.16339/j.cnki.hdxbzkb.2018.02.01.
[34] F. Chaari, T. Fakhfakh and M. Haddar, Analytical modelling of spur gear tooth crack and influence on gearmesh stiffness, European Journal of Mechanics-A/Solids. 28 (2009) 461 – 468, https://doi.org/10.1016/j.euromechsol.2008.07.007.
[35] P. Sainsot And, P. Velex and O. Duverger, Contribution of gear body to tooth deflections—a new bidimensional analytical formula, J. Mech. Des. 126 (2004) 748 – 752, https://doi.org/10.1115/1.1758252.
[36] S. Li , J. Yang , J.Zhang, Preliminary application of KL expansion in random analysis of seepage fields, Yangtze river scientific research institute bulletin. 26 (2009) 39 – 43.
[37] J. Wen, J. Du, K. Liu , Z. Wang, Analysis of the dynamic characteristics of high-speed ship propulsion bevel gears considering time-varying meshing stiffness, Journal of Xi'an university of technology. 35 (2019) 80 – 85+126, http://doi.org/10.19322/j.cnki.issn.1006-4710.2019.01.013.
[38] J. Pei, Y. Tian, H. Hou, Y. Tao, M. Wu and Z. Guan, Dynamic response and lubrication performance of spur gear pair under time-varying rotation speeds, Lubricants. 13 (2025) 15, https://doi.org/10.3390/lubricants13010015.

Author Contributions

All authors contributed to the study conception and design. Material preparation, data collection, and analysis were performed by Shaopeng Guan, Jiaxing Pei, and LeiLei Wang. The first draft of the manuscript was written by Shaopeng Guan, and Hongjuan Hou, Yipeng Zhao, and Ruisheng Hou commented on previous versions of the manuscript. The study was supervised by Jiaxing Pei, and funding acquisition was carried out by Lingwei Kong and Jianing Cao. All authors read and approved the final manuscript.

Competing Interests

The authors declare that they have no conflict of interest.

Funding

This work is supported by the Scientific research projects of higher education institutions in Hebei Province (Grant numbers QN22026296).

Data Availability

The datasets generated and/or analysed during the current study are not publicly available because the associated project and related research are still ongoing but are available from the corresponding author on reasonable request.